

# Growth of Carbon Nanotubes inside Boron Nitride Nanotubes by Coalescence of Fullerenes: Toward the World's Smallest Coaxial Cable

Kate E. Walker, Graham A. Rance,\* Áron Pekker, Hajnalka M. Tóháti, Michael W. Fay, Rhys W. Lodge, Craig T. Stoppiello, Katalin Kamarás, and Andrei N. Khlobystov\*

The use of boron nitride nanotubes as effective nanoscale containers for the confinement and thermal transformations of molecules of C<sub>60</sub>-fullerene is demonstrated. The gas-phase insertion of fullerenes into the internal channel of boron nitride nanotubes yields quasi-1D arrays, with packing arrangements of the guest fullerenes different from those in the bulk crystal and critically dependent on the internal diameter of the host nanotube. Interestingly, the confined fullerene molecules: i) exhibit dynamic behavior and temperature-dependent phase transitions analogous to that observed in the bulk crystal, and ii) can be effectively removed from within the internal channel of nanotubes by excessive sonication in organic solvent, indicating weak host–guest interactions. The thermal treatment of fullerenes confined within nanotubes at 1200 °C in argon triggers the polymerization and coalescence of the guest fullerenes into carbon nanotubes inside boron nitride nanotubes affording a hybrid nanostructure—the world's smallest coaxial cable—on a preparative scale, as confirmed by high-resolution bright-field transmission electron microscopy imaging, electron-energy-loss spectroscopy, energy-filtered transmission electron microscopy elemental mapping, and UV–vis absorption spectroscopy.


## 1. Introduction

Carbon nanotubes (CNTs) are hollow, 1D containers, with high tensile strength,<sup>[1]</sup> chemical stability,<sup>[2]</sup> and electrical conductivity.<sup>[3]</sup> Described as the world's smallest test tube, they behave

K. E. Walker, R. W. Lodge, Dr. C. T. Stoppiello, Prof. A. N. Khlobystov  
School of Chemistry  
University of Nottingham  
University Park, Nottingham NG7 2RD, UK  
E-mail: Andrei.Khlobystov@nottingham.ac.uk

Dr. G. A. Rance, Dr. M. W. Fay  
Nanoscale and Microscale Research Centre, Cripps South  
University of Nottingham  
University Park, Nottingham NG7 2RD, UK  
E-mail: Graham.Rance@nottingham.ac.uk

Dr. Á. Pekker, H. M. Tóháti, Prof. K. Kamarás  
Institute for Solid State Physics and Optics  
Wigner Research Centre for Physics  
Hungarian Academy of Sciences  
Konkoly-Thege M. 29-33, 1121 Budapest, Hungary

 The ORCID identification number(s) for the author(s) of this article can be found under <https://doi.org/10.1002/smt.201700184>.

DOI: 10.1002/smt.201700184

as excellent nanoscale containers for molecules,<sup>[4–6]</sup> metals,<sup>[7–9]</sup> and metal halides,<sup>[10]</sup> where the spontaneous encapsulation is driven by van der Waals forces that stabilize the confined guest species in the internal channel of the host nanotube.<sup>[11]</sup> Moreover, a good geometric fit between the critical dimensions of the encapsulated guest and the internal dimensions of the host can result in van der Waals forces that are sufficiently high that insertion is irreversible. This effective nanoscale confinement permits the study of the structure,<sup>[12,13]</sup> motion,<sup>[14]</sup> and dynamics<sup>[15,16]</sup> of individual molecules.

Furthermore, extreme spatial confinement in CNTs allows us to probe the kinetics and pathways of chemical reactions and processes at the nanoscale, including the formation of 1D materials templated by the internal channel of the host nanotube.<sup>[6,17,18]</sup> The simplest and most widely studied confined trans-

formation in single-walled carbon nanotubes (SWCNTs) is the conversion of C<sub>60</sub>@SWCNT, so-called “peapods,” into double-walled carbon nanotubes (DWCNTs) via the thermally activated polymerization and coalescence of guest fullerenes to an internal carbon nanotube.<sup>[17,19]</sup> Numerous more complex processes have also been observed inside nanotubes, such as unusual oligomerization and polymerization reactions,<sup>[13,20,21]</sup> the growth of graphene nanoribbons,<sup>[22–24]</sup> and the formation of molecular nanodiamonds<sup>[18]</sup> from encapsulated fullerenes and organic molecules, respectively. As such, chemical reactions inside carbon nanotubes open up new avenues for the synthesis of nanoscale materials with unique structures and functional properties inaccessible by other means.

Boron nitride nanotubes (BNNTs) are isoelectronic to CNTs and similarly possess high mechanical strength<sup>[25]</sup> and excellent chemical and thermal stabilities.<sup>[26]</sup> In contrast to CNTs, however, BNNTs are electronically insulating, a consequence of the partly ionic interatomic B–N bonding, and optically transparent with a wide bandgap.<sup>[27,28]</sup> While less well explored relative to CNTs, BNNTs represent a remarkable class of 1D nanoscale containers for metals,<sup>[29–34]</sup> metal halides,<sup>[35,36]</sup> and molecules, such as C<sub>60</sub>,<sup>[37]</sup> and owing to their transparency to visible light

offer the opportunity to probe the photochemistry of encapsulated molecules. Like CNTs, the encapsulation of guest species into BNNTs is modulated by ubiquitous van der Waals forces between host and guest.<sup>[38]</sup> Yet, as the polarity of interatomic bonding, delocalization of  $\pi$  electrons and polarizability differ significantly between CNTs and BNNTs, the extent to which these properties can influence the interactions between BNNTs and molecules are at present not fully understood. Moreover, experimental studies on the structure, motion, dynamics, and reactivity of molecules in BNNTs are still extremely limited, particularly those that afford hybrid nanostructures on the preparative scale, with one rare example being the formation of metal particles from metal halides.<sup>[36]</sup>

Here, we make the first important steps toward establishing BNNTs as a nanoreactor through the thermally assisted polymerization and coalescence of  $C_{60}$ , a classical model reaction in CNTs, as a test reaction for BNNT nanoreactors. The interactions of  $C_{60}$  with BNNTs and intermolecular reactions of  $C_{60}$  inside the nanotube demonstrate the ability of BNNTs to act as an effective template of 1D nanostructures, ultimately leading to the formation of CNT@BNNT, where an electrically conducting CNT is embedded within an insulating BNNT. Such a nanostructure—the world's smallest coaxial cable—affordable using our approach on a preparative scale is predicted to have a wealth of unique functional properties for applications in nano-electronics and sensing devices.<sup>[39–41]</sup>

## 2. Results and Discussion

A fundamental requirement for the transfer of any guest species into the inner cavity of a host nanotube is the presence of accessible holes through which the guests can pass. Our transmission electron microscopy (TEM) observations (see Figure S1, Supporting Information) indicate that while the internal diameter of BNNTs ( $d_{\text{int}} = 2.45 \pm 1.19$  nm) is large enough to accommodate  $C_{60}$  (van der Waals diameter  $d_{\text{vdW}} = 1.0$  nm), most nanotubes are capped and possess a moderate amount of boron-containing impurities which will prohibit the transport of  $C_{60}$  into the inner channel. Therefore, the first challenge in our multistep synthetic strategy (Figure 1) was to develop a reliable method for opening and purifying BNNTs.

A variety of different methods have been reported for the selective opening of BNNTs.<sup>[42–45]</sup> We have tested: i) oxidation in air (Method 1), ii) ball milling (Method 2), and iii) hydrolysis followed by oxidation in air (Method 3a–c) for the controlled opening and purification of BNNTs, and found Method 3a to be the most effective (Table 1, and Figure S2–S4, Supporting Information).

In Method 3, the lone pair of electrons on the N atom of the ammonia molecules interacts with the empty  $p_z$  orbital of B in the as-received BNNTs, activating B–N bonds toward hydrolysis and causing the corrosion, thinning, and removal of the BNNT end caps. The end caps typically contain strained four- or eight-membered rings,<sup>[46,47]</sup> making them more susceptible to reaction with water

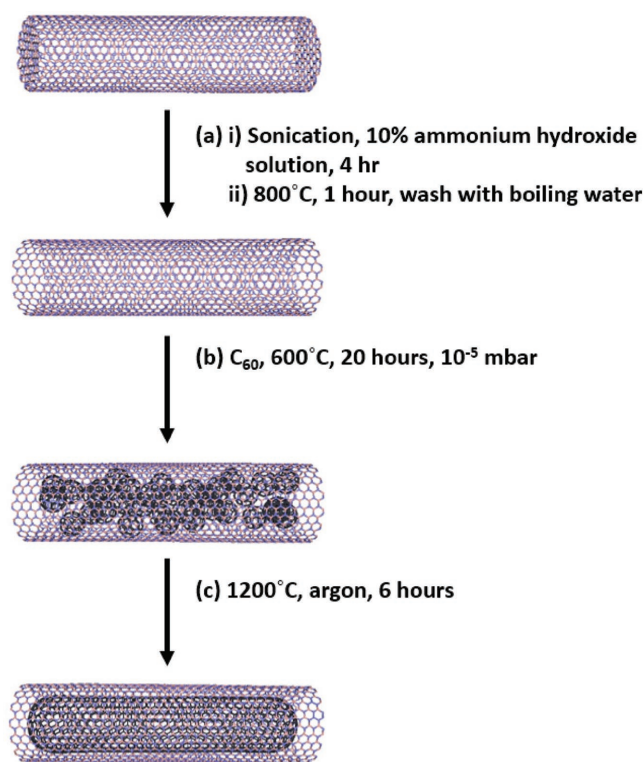


**Figure 1.** The multistep method used to produce CNT@BNNT: a) the opening and purification of BNNTs, b) the encapsulation of  $C_{60}$  into BNNTs, and c) the transformation of  $C_{60}$  to CNTs in BNNTs.

molecules than the less strained six-membered rings forming the sidewalls and thus are selectively removed. The resultant BNNTs are terminated with either ammonia, or hydroxyl groups as a result of hydrolysis, causing them to be more hydrophilic and dispersible in water. A significant reduction in the mean length from over 200 to  $0.55 \pm 0.22$   $\mu\text{m}$ , essential for minimization of the expected length-dependent transport resistance of guest molecules within the host nanotube,<sup>[48]</sup> as measured by TEM was determined through statistical analysis of multiple microscopy images, and the resulting BNNTs are free of the boron impurities as confirmed by energy-dispersive X-ray (EDX) spectroscopy. Most importantly, the BNNTs subsequent to this treatment are open, as well as shorter and purer, making them suitable for filling with guest molecules.

**Table 1.** Comparison of methods for opening and purifying BNNTs.

Method	Conditions	LNT <sup>a)</sup> [ $\mu\text{m}$ ]	% open <sup>a)</sup>	B:N <sup>b)</sup>
–	As-received	>200	<1	61:39
1	Oxidation in air (800 °C, 1 h)	>200	<1	87:13
2	Ball milling (10 Hz, 90 min)	$1.98 \pm 0.78$	80	57:43
3a	Hydrolysis (4 h), oxidation in air (800 °C, 1 h)	$0.55 \pm 0.22$	83	51:49
3b	Hydrolysis (10 h), oxidation in air (800 °C, 1 h)	$0.16 \pm 0.05$	81	55:45
3c	Hydrolysis (24 h), oxidation in air (800 °C, 1 h)	$0.14 \pm 0.06$	88	55:45

<sup>a)</sup>Determined by statistical analysis of TEM images; <sup>b)</sup>Determined by EDX spectroscopy.

The encapsulation of  $C_{60}$  into BNNTs was carried out at 600 °C in vacuum which is based on an effective method for the preparation of  $C_{60}@CNT$ .<sup>[12]</sup> The encapsulation of  $C_{60}$  into CNTs is known to be a highly exothermic and generally irreversible process (up to 3 eV per  $C_{60}$ , depending on the specific van der Waals contact area between the convex external surface of  $C_{60}$  and the concave internal surface of the CNT channel),<sup>[49,50]</sup> in which adsorbed  $C_{60}$  migrates along the surface of the CNT before entering at the termini and at accessible defect sites along the sidewall. Provided the CNT diameter is large enough to accommodate  $C_{60}$  molecules (0.6 nm wider than the diameter of the guest molecule), the CNTs will be completely filled.<sup>[12,51,52]</sup> While the encapsulation of  $C_{60}$  into BNNTs has been reported,<sup>[37]</sup> no experimental studies to date report the energy of encapsulation of  $C_{60}$  into BNNTs. However, the calculated energy of adsorption for  $C_{60}$  onto graphene (0.85 eV) is comparable to  $C_{60}$  onto hexagonal boron nitride sheets (0.83 eV),<sup>[50]</sup> suggesting similar interactions for  $C_{60}@BNNT$  and  $C_{60}@CNT$ .<sup>[53]</sup> Moreover, the calculated energy for encapsulation into CNTs and BNNTs suggests that the energy gain for the insertion of  $C_{60}$  into BNNTs ( $C_{60}@ (10, 10)BNNT$   $\Delta E = 4.38$  eV) may surpass that of the CNT analogue ( $C_{60}@ (10, 10)CNT$   $\Delta E = 3.02$  eV).<sup>[38]</sup>

TEM imaging confirms the filling of BNNTs under our conditions (Figure 2). Similar to CNTs with internal diameters matching the van der Waals diameter of  $C_{60}$ , the guest molecules of  $C_{60}$  confined within narrow BNNTs line up in a single chain, with separations of  $\approx 0.3$  nm between the neighboring fullerenes and between the fullerene and the internal walls of BNNTs (Figure 2a). The interfullerene distance is  $\approx 0.9$ –1.0 nm (depending on the diameter of the host nanotube), consistent with a previous study of  $C_{60}$  in BNNTs<sup>[37]</sup> and the minimum separation in the bulk fcc crystal (1.0 nm)<sup>[54,55]</sup> and slightly smaller than in SWCNTs (1.1 nm)<sup>[48]</sup> as a result of tighter packing arrangements. These measurements indicate that the nature of  $C_{60}$ –BNNT interactions is similar to that of  $C_{60}$ –CNT interactions.

In wider BNNTs, fullerenes adjust their positions to maximize the interactions with the host nanotube and to fill the cylindrical cavity in the most efficient way (Figure 2b–d, and Figure S5, Supporting Information), which is analogous to the behavior of  $C_{60}$  in wider CNTs.<sup>[12]</sup> This forms packing patterns of  $C_{60}$  which are clearly ordered in some cases (Figure 2a,c), but more disordered in others (Figure 2b,d). For example, there is no real packing order in the very large BNNT in Figure 2d possibly due to the wide, yet variable, diameter of BNNT in this instance. Figure 2c appears to show a corkscrew arrangement of  $C_{60}$  inside the BNNT with an internal diameter of 2.6 nm which agrees with previous studies of  $C_{60}$  in BNNTs,<sup>[37]</sup> but some other corkscrew packing patterns, such as in Figure 2b appear to be discontinuous along the length of the nanotube, possibly due to the nonuniform diameter of the host BNNT. Nonhelical packing patterns are also present (Figure 2a), such as the two-molecule layer phase inside a 2.1 nm diameter BNNT, narrower than that described for  $C_{60}$  inside an  $\approx 2.6$  nm DWCNT.<sup>[12]</sup> Statistical analysis of multiple electron microscopy images indicated that around 25% of the BNNTs are completely filled.

To further probe the efficiency of encapsulation of  $C_{60}$  in BNNTs, IR and UV–vis spectroscopy were performed (Figure 3).

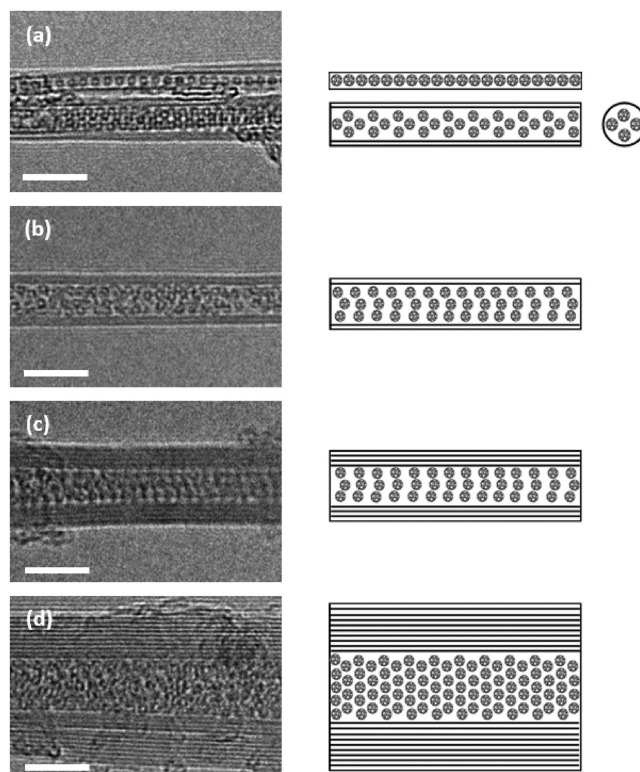


**Figure 2.** TEM images and schematic representations of  $C_{60}@BNNT$  demonstrating the dependence of the stacking arrangement of  $C_{60}$  on the internal diameter of the respective BNNT: a) 1.2 nm (top), 2.1 nm (bottom), b) 2.4–2.6 nm, c)  $\approx 2.6$  nm, and d) 4.4–5.2 nm. The stacking arrangements are assigned to a) linear (top), two-layer phase (bottom), b) helical, c) helical, and d) amorphous. The schematic representations indicate the possible stacking arrangements of  $C_{60}$  inside BNNTs of uniform diameter. Scale bars are 5 nm.

Being electrically insulating and optically transparent, BNNTs should allow the vibrations of guest molecules to be directly analyzed by IR spectroscopy, unlike CNTs that have often hindered such analysis.<sup>[56]</sup> Indeed, the IR spectrum of toluene-washed  $C_{60}@BNNT$  (Figure 3a) contains prominent bands at 803 and 1375  $cm^{-1}$  corresponding to the out-of-plane radial buckling (R) mode and the in-plane stretching modes of h-BN in BNNTs, respectively,<sup>[57,58]</sup> as well as weak features at 527, 576, and 1183  $cm^{-1}$  consistent with known vibrational modes of  $T_{1u}(1)$ ,  $T_{1u}(2)$ , and  $T_{1u}(3)$  symmetry in  $C_{60}$ .<sup>[59]</sup> Through correlation of the dependence of the absorbance intensity at 527  $cm^{-1}$  ( $T_{1u}(1)$ ) with the mass of  $C_{60}$  (Figure 3b,c), the quantity of  $C_{60}$  in  $C_{60}@BNNT$  was found to be  $\approx 29$  mass%. Corresponding UV–vis spectroscopy analysis (Figure 3d–f) indicated that the amount of  $C_{60}$  extracted from  $C_{60}@BNNT$  through extensive sonication in toluene was  $\approx 37\%$ . The slight differences in loading of  $C_{60}$  inside BNNTs obtained by different spectroscopic methods can be readily attributed to the wide distribution of BNNT diameters present within a given sample.

It is important to note that both the IR spectroscopy method, where  $C_{60}$  remains within the internal channel of BNNTs during analysis, and the UV–vis spectroscopy approach, where  $C_{60}$  has been removed, give approximately the same loading of  $C_{60}$  in BNNTs as was observed by TEM analysis. Moreover, comparison



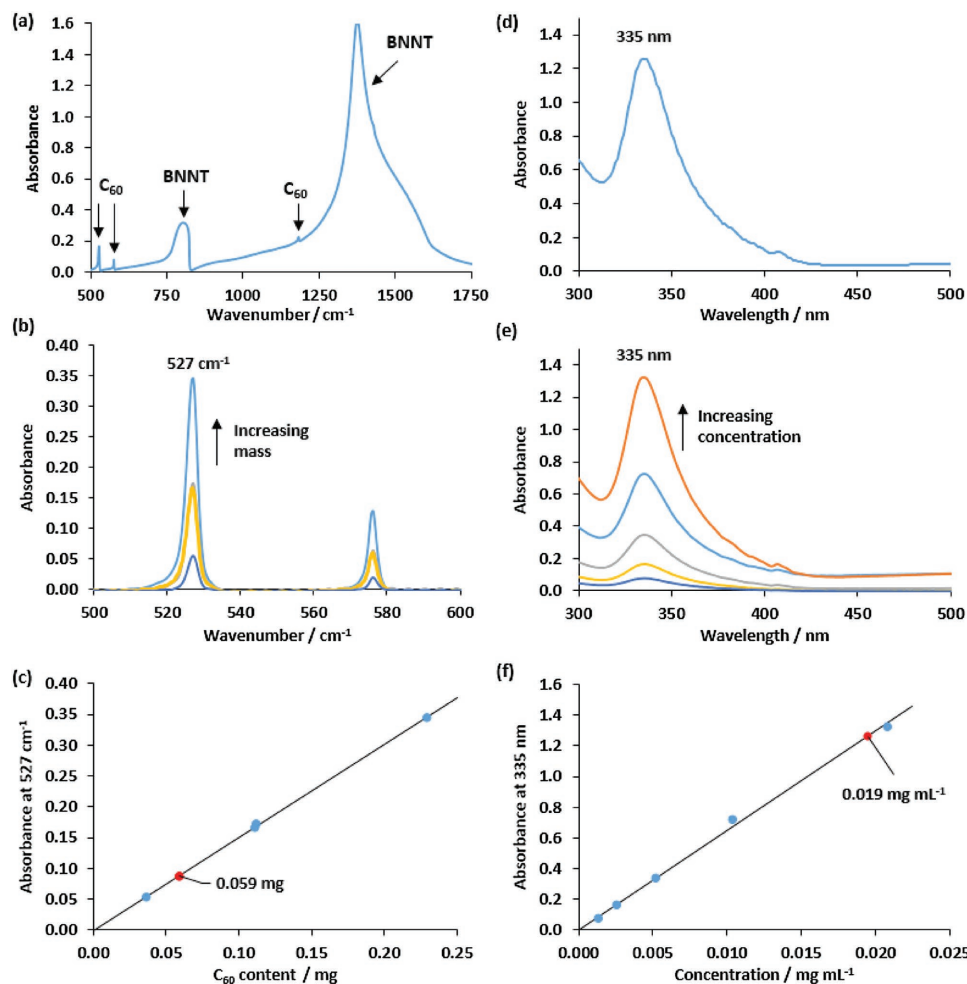


**Figure 3.** a) IR spectrum of  $C_{60}$ @BNNT. b,c) Baseline-corrected IR spectra of  $C_{60}$  with varying  $C_{60}$  content (0.036, 0.111, 0.112, and 0.230 mg) in potassium bromide (265 mg) (b) used to construct the calibration curve (c), which correlates the intensity of the absorbance at  $527\text{ cm}^{-1}$  ( $T_{1u}(1)$ ) with  $C_{60}$  content. The amount of  $C_{60}$  in  $C_{60}$ @BNNT using this method was found to be 0.059 mg in 0.260 mg (mass ratio  $\approx 29\%$ ).  $\gamma = 1.509x$ ,  $R^2 = 1.000$ , standard error = 0.01. d) UV-vis spectrum of  $C_{60}$  extracted from  $C_{60}$ @BNNT through extensive sonication in toluene (4 mL). e,f) UV-vis spectra of  $C_{60}$  at a variety of concentrations in toluene (0.0013, 0.0026, 0.0052, 0.0104, and 0.0208 mg  $\text{mL}^{-1}$ ) (e) used to produce the calibration curve (f), which correlates the intensity of the absorbance at 335 nm with the concentration of  $C_{60}$  in toluene. The amount of  $C_{60}$  extracted from  $C_{60}$ @BNNT using this method was found to be 0.019 mg in 0.07 mg (mass ratio  $\approx 37\%$ ).  $\gamma = 64.7x$ ,  $R^2 = 0.998$ , standard error = 1.15.

of the spectroscopy approaches confirms that  $C_{60}$  can be effectively removed from within BNNTs by excessive sonication in organic solvent (toluene), a feat that cannot be achieved from within CNTs. This suggests that the host-guest interactions in  $C_{60}$ @BNNT are likely to be weaker than in  $C_{60}$ @CNT; however, the poor host-guest fit (the van der Waals diameter of  $C_{60}$  of 1.0 nm is smaller than the mean internal diameter of BNNTs of  $2.45 \pm 1.19$  nm) precludes a large number of  $C_{60}$ -BNNT contacts and as such the encapsulated fullerenes can be solvated in a manner analogous to that observed in the bulk fcc crystal. This observation also indicates that caution has to be exercised when purifying the products: repeated rinsing with toluene should be used for removing  $C_{60}$  molecules from the surface but sonication should be avoided as it results in emptying the BNNTs.

Temperature-dependent IR spectroscopy was used to identify the different vibrational modes of guest molecules of  $C_{60}$  inside BNNTs as orientational order develops with the lowering of the temperature (Figure 4).

At 300 K, the spectrum of  $C_{60}$  in  $C_{60}$ @BNNT contains only the four IR-active  $T_{1u}$  modes of the icosahedral  $C_{60}$  molecule. As the temperature decreases below the orientational phase transition temperature, the molecular rotation is restricted leading to a lowering of the symmetry as the molecules have to adjust to the crystal structure. This results in splitting of the triply degenerate  $T_{1u}$  modes and the appearance of previously IR-inactive new modes (Figure 4a). The new bands at  $712.1$  and  $739.6\text{ cm}^{-1}$  (Figure 4b), assigned to  $H_u$  symmetry,<sup>[60]</sup> increase in intensity with decreasing temperature (Figure 4c). The temperature where they appear is around 250 K, exactly where the orientational phase transition occurs in fcc  $C_{60}$ .<sup>[54]</sup> Splitting of the  $T_{1u}$  modes, such as the  $526.7\text{ cm}^{-1}$  band ( $T_{1u}(1)$ ) becoming two at  $525.9$  and  $526.6\text{ cm}^{-1}$  (Figure 4d) and the  $1428.3\text{ cm}^{-1}$  band ( $G_u/T_{1u}(4)$ ) splitting into three bands at  $1427.9$ ,  $1431.0$ , and  $1431.5\text{ cm}^{-1}$  (Figure 4f), along with the lack of splitting of the  $T_{1u}(3)$  mode (Figure 4e), are also consistent with earlier observations in the bulk fcc crystal.<sup>[59]</sup> This temperature-dependent

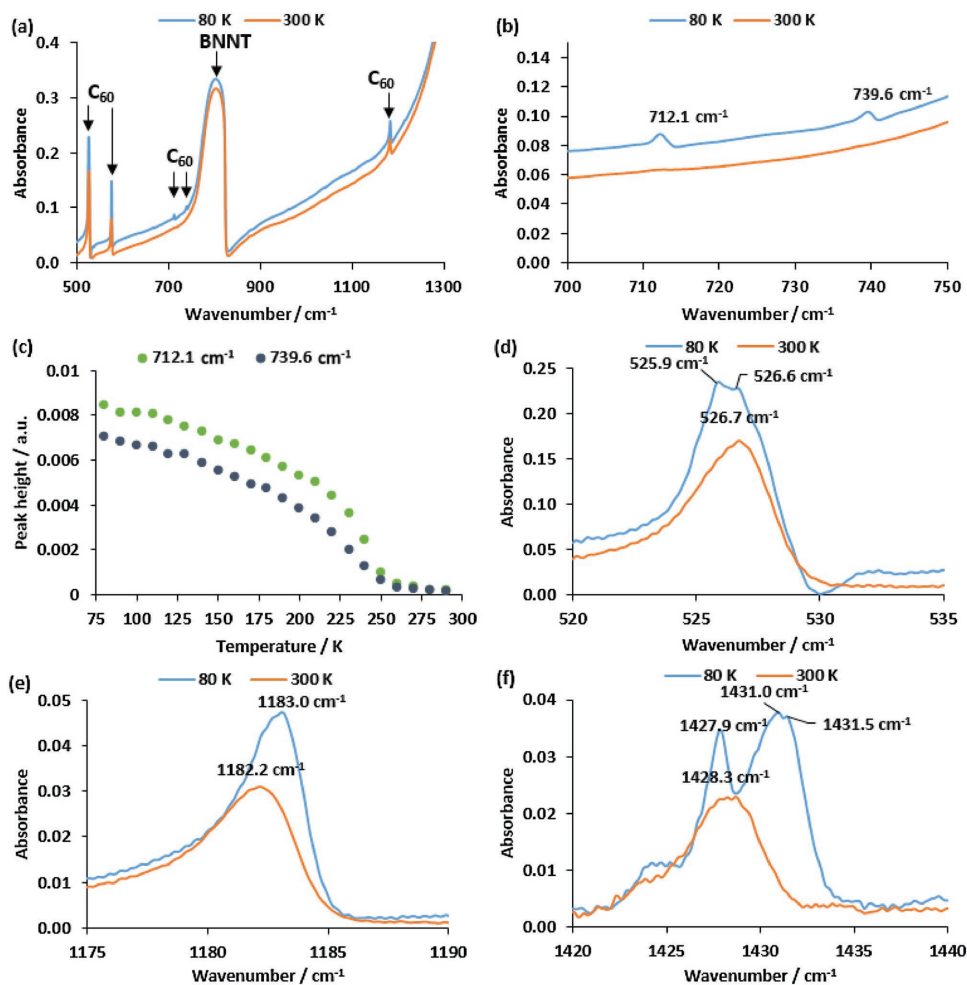


**Figure 4.** a,b) High-resolution IR spectra of  $C_{60}$ @BNNT at 80 and 300 K in the ranges 500–1300  $cm^{-1}$  (a) and 700–750  $cm^{-1}$  (b). c) The heights of the peaks at 712.1 and 739.6  $cm^{-1}$  ( $H_u$ ) vary as a function of temperature. d–f) The band at 526.7  $cm^{-1}$  ( $T_{1u}(1)$ ) increases in intensity and splits into two peaks at 525.9 and 526.6  $cm^{-1}$  (d), the band intensity at 1182.2  $cm^{-1}$  ( $T_{1u}(3)$ ) increases and shifts to higher energy (e), and the band at 1428.3  $cm^{-1}$  ( $G_u/T_{1u}(4)$ ) splits into three bands when cooled from 300 to 80 K (f).

behavior suggests that  $C_{60}$  molecules are in a similar environment when encapsulated in the BNNTs. Vibrational spectroscopy, however, reflects short-range rather than long-range order: The lowering of symmetry indicates that the molecular rotation has stopped due to interaction with neighboring fullerenes. The orientational transition temperature is determined by the intermolecular distance<sup>[61]</sup> rather than the long-range crystal structure; so long as the intermolecular distance is similar, these results can be reconciled with any arrangement shown in Figure 2.

The presence of  $C_{60}$  is also proven by Raman spectroscopy (see Figure S6, Supporting Information). Five of the ten Raman-active modes can be clearly identified in the Raman spectrum of  $C_{60}$ @BNNT.<sup>[62]</sup> We regard this as sufficient, as the remaining modes have small intensity. Encapsulation does not cause a measurable shift in the frequency of these vibrational modes, unlike what has been reported for narrow-diameter carbon nanotube peapods.<sup>[63]</sup> However, such behavior was observed in carbon nanotube peapods with a large mean diameter and a broad diameter distribution, similar to our BNNTs.<sup>[64]</sup>

The polymerization and coalescence of guest  $C_{60}$  molecules into a CNT inside the host BNNT offer an exciting opportunity to form a conducting nanowire inside an insulating BNNT. Previous attempts to fabricate CNT@BNNT have been made by other routes, such as the coating of CNT with boron nitride.<sup>[65–72]</sup> However, the formation of CNTs within preformed BNNTs would be more desirable because the structure of the outer insulating nanotube is well-defined and easier to control with uniform coverage of BN. Furthermore, this approach also permits the formation of very narrow SWCNTs in BNNTs, a nanostructure with favorable properties in chemical sensing.<sup>[73]</sup> Two noteworthy examples of forming CNT@BNNT using preformed BNNTs involve the electron irradiation of amorphous carbon<sup>[74]</sup> and  $C_{60}$ <sup>[37]</sup> inside BNNTs, though the inherent nature of this method is not scalable.

Previous studies on the thermal transformations of  $C_{60}$ @CNT suggest that confined  $C_{60}$  molecules begin to coalesce at  $\approx 800$  °C inside a CNT,<sup>[19]</sup> and at 1200 °C most of the  $C_{60}$  has rearranged to form an internal CNT within the host CNT.<sup>[75]</sup> The templating effects of the host CNT were shown to be

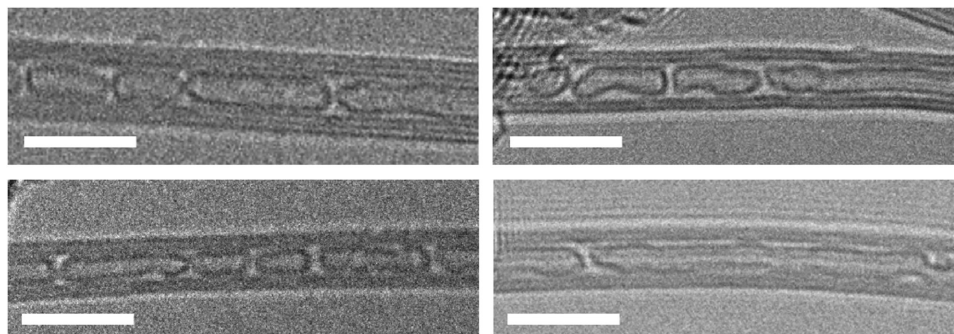


**Figure 5.** Bright-field TEM images of CNT@BNNT formed from C<sub>60</sub>@BNNT at 1200 °C. Scale bars are 5 nm.

important in the CNT formation, as the diameter of the inner CNT is dependent on the outer nanotube and completely independent of the size of C<sub>60</sub>.<sup>[19]</sup> In our study, we heated C<sub>60</sub>@BNNT at 1200 °C for 6 h under argon to stimulate the polymerization and coalescence processes, similar to those well documented for C<sub>60</sub>@CNT. The method was varied through several approaches (see Table S1, Figure S9–S11, Supporting Information), yet did not show any clear benefits. During the heating process, C<sub>60</sub> desorbs from within the wider (>2 nm diameter) BNNTs, and as such CNTs are only formed in narrow BNNTs, consistent with the previously reported desorption of C<sub>60</sub> from wider CNT.<sup>[76]</sup> Furthermore, thermogravimetric analysis (TGA) measurements in air of C<sub>60</sub>@BNNT after heating at 1200 °C in argon show a reduction in the carbon content of the material by a factor of four, from around 8% of C in C<sub>60</sub>@BNNT before heating (see Figure S7, Supporting Information) to around 2% after (see Figure S8, Supporting Information). It is likely that larger nanotubes, with lower host–guest contact area and hence weaker van der Waals interactions between the fullerene and the BNNTs, cannot retain C<sub>60</sub> inside the nanotube and as such some of the confined material becomes lost during heating.

The Raman spectrum of C<sub>60</sub>@BNNT shows clear changes on thermal annealing (see Figure S12, Supporting Information): the C<sub>60</sub> modes disappear and those of carbon nanotubes (the D and G modes at around 1300 and 1600 cm<sup>-1</sup>, respectively) are observed. The growth of inner nanotubes proves that the majority of C<sub>60</sub> molecules were encapsulated.

TEM imaging of C<sub>60</sub>@BNNT after heating reveals that most molecules have undergone coalescence to tubular structures with mean diameters of 1.1 ± 0.2 nm and lengths of 4.3 ± 2.9 nm, with a modal van der Waals separation of ≈0.34 nm between the CNT and BNNT (Figure 5).

To confirm that the cylindrical structures observed in the TEM images of CNT@BNNT are in fact carbon nanotubes encapsulated in boron nitride nanotubes, the sample was analyzed by electron-energy-loss spectroscopy (EELS) and energy-filtered TEM (EFTEM) imaging, which maps the location of each element within this hybrid nanomaterial (Figure 6).

The linear contrast showing the location of carbon in the CNT@BNNT structure is visibly narrower (3.2 nm) than those attained for boron (3.9 nm) and nitrogen (3.9 nm), providing further evidence that the structures are indeed CNTs embedded within BNNTs. Since BNNTs are electrical insulators, charge induced by the e-beam during TEM analysis builds up and

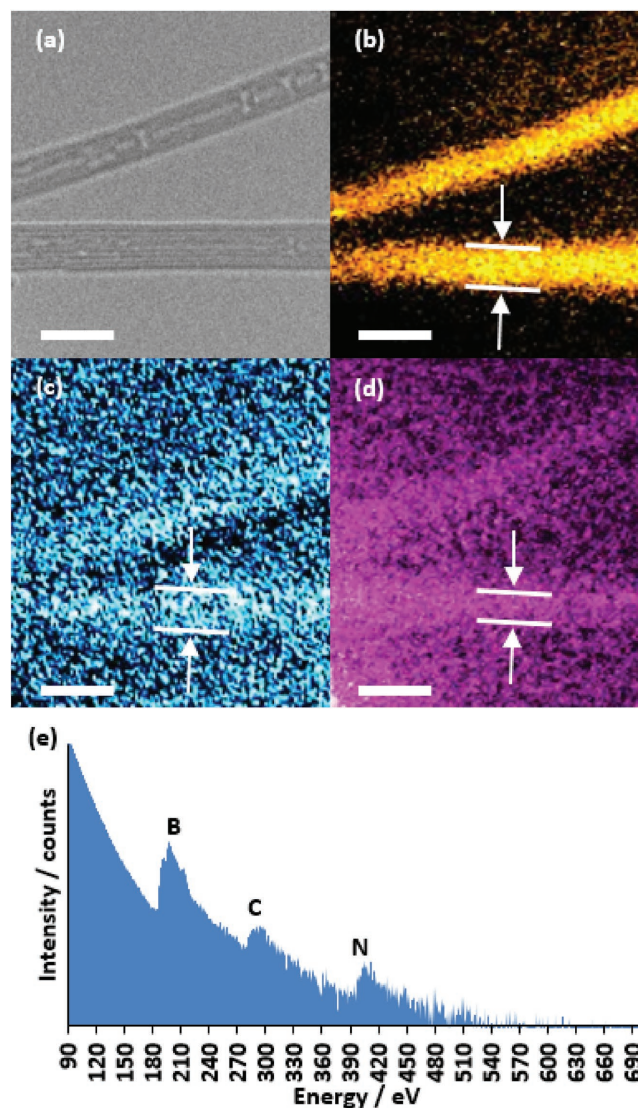


**Figure 6.** a) Bright-field TEM image of CNT@BNNT produced by heating C<sub>60</sub>@BNNT. b–d) EELS and EFTEM elemental maps showing the distributions of boron (b), nitrogen (c), and carbon (d) in the same nanotube. The line widths for boron, carbon, and nitrogen are 3.9, 3.2, and 3.9 nm, respectively. e) A representative electron energy loss spectrum of CNT@BNNT. Scale bars are 5 nm.



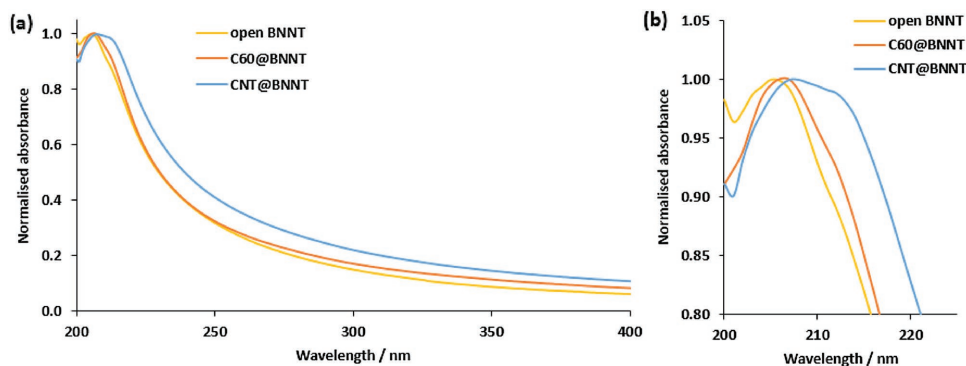


**Figure 7.** a) UV-vis spectra of open and purified BNNTs, C<sub>60</sub>@BNNT, and CNT@BNNT. The experimentally determined bandgaps are 6.04 eV (205.3 nm) for open and purified BNNTs, 6.00 eV (206.5 nm) for C<sub>60</sub>@BNNT, and 5.98 eV (207.4 nm) for CNT@BNNT. b) A shoulder at 212 nm in the spectrum of CNT@BNNT is consistent with the  $\pi$ - $\pi^*$  absorption of a narrow SWCNT.

cannot be removed from the sample. This causes the BNNTs to move around, thus blurring EFTEM images during the data acquisition, such as in the case of upper CNT@BNNT in Figure 6 which appears broader as a result. The bottom nanotube in Figure 6, however, is fixed firmly at both ends on the TEM grid, restricting the movement and producing clearer elemental maps. It is also worth noting that with B:N = 1:1, the nitrogen signal will appear much weaker than the boron signal, as the relationship between core-loss intensity and energy is approximately that of an inverse power law.<sup>[77]</sup>

UV-vis spectroscopy is used as a tool to understand the size of the electronic bandgap of the new material CNT@BNNT (Figure 7).

The absorption maximum shifts to a higher wavelength as the BNNT is opened and purified, filled with C<sub>60</sub> and then finally transformed into CNT@BNNT. For CNT@BNNT, the electronic structures of the BNNTs and CNTs in the composite are predicted to change when compared to the pristine nanotube analogues due to the stretching of C-C bonds and compression of B-N bonds,<sup>[78]</sup> explaining our measured change in the bandgap of BNNTs when the CNT is encapsulated. However, the BNNTs will remain insulating and the CNT core will be electronically conducting.<sup>[78]</sup> The most significant result from the UV-vis spectroscopy measurements is that the absorption band of CNT@BNNT is significantly broader than for any other samples and has a distinct shoulder at 212 nm (Figure 7b), which corresponds to the  $\pi$ - $\pi^*$  excitation of a single-walled carbon nanotube with a diameter of 0.90 nm.<sup>[79]</sup> This value is consistent with the diameter of a carbon nanotube formed from C<sub>60</sub> inside BNNTs measured in TEM images of CNT@BNNT (0.9–1.2 nm at the widest point, with narrow parts of as small as 0.4 nm).

### 3. Conclusion

Boron nitride nanotubes have been demonstrated as effective nanoscale containers and reactors for molecules of fullerene C<sub>60</sub> which can be inserted into BNNTs from the gas phase to form ordered quasi-1D arrays. The packing arrangement of fullerenes in C<sub>60</sub>@BNNT was shown to be different to the packing of C<sub>60</sub> in the bulk crystal and highly dependent on the internal

diameter of the host nanotube, but IR spectroscopy analysis of the guest molecules suggests that the dynamic behavior and temperature-controlled phase transitions of C<sub>60</sub> in BNNTs are the same as in the bulk fullerene crystal. The thermal treatment of C<sub>60</sub>@BNNT at 1200 °C in argon triggers drastic transformations of the guest molecules which polymerize and coalesce into carbon nanotubes inside boron nitride nanotubes thus forming a hybrid nanostructure CNT@BNNT, as confirmed by high-resolution bright-field TEM imaging and EELS and EFTEM elemental mapping of individual CNT@BNNT structures, which suggests that B and N comprise the shell and C is located in the core of this hybrid nanostructure. Furthermore, UV-vis absorption spectroscopy indicates a new optical transition in CNT@BNNT material (absent in BNNTs or C<sub>60</sub>@BNNT) suggesting that the average diameter of the guest carbon nanotube is  $\approx$ 0.9 nm which correlates well with that measured by TEM. Overall, the concentric structure CNT@BNNT with insulating BNNTs as the outer shell, and conducting CNTs as the inner core, represents an excellent candidate material for nanoscale coaxial cables which are required for several electronic and sensing applications.<sup>[39–41]</sup> Our method of carbon nanotube growth from molecules, directly inside BNNTs, builds on the concept of nanoreactors we developed for carbon nanotubes, and provides the first scalable method for the controlled growth of conducting nanotubes inside insulating nanotubes.

### 4. Experimental Section

*General Experimental:* All common reagents and solvents were purchased from Sigma-Aldrich, UK, and used without further purification unless stated otherwise. Water was purified (>18.0 M $\Omega$  cm) using a Barnstead NANOpure II system. TEM imaging was performed using a JEOL 2100F TEM (field emission gun source, information limit <0.19 nm) at 100 kV at room temperature. EEL spectra were acquired using a Gatan Tridiem energy filter from regions defined by the selected area aperture to exclude any contribution from the supporting carbon film. Acquisition parameters were a 2 mm spectrometer aperture, with a dispersion of 0.3 eV per pixel. The line widths for boron, carbon, and nitrogen in EELS and EFTEM elemental maps were determined by fitting the intensity profile in Digital Micrograph software. EDX spectra were recorded using an Oxford Instruments 30 mm<sup>2</sup> Si(Li) detector or an Oxford Instruments x-Max 80 SDD running on an INCA microanalysis system. Samples for TEM, EELS, and EDX

were typically prepared by casting several drops of a suspension of nanotubes onto copper-grid mounted “lacy” carbon films. Raman spectroscopy was conducted using a laser wavelength of 355 nm. FTIR spectroscopy was performed on a Bruker IFS66v spectrometer using the KBr pellet technique. UV–vis spectroscopy was performed using an Ocean Optics QE65000 spectrometer or Perkin-Elmer Lambda 25 UV–vis spectrometer. TGA was performed using a TA Instruments SDT Q600 under a flow of air at a heating rate of 10 °C min<sup>-1</sup> from room temperature to 1000 °C. Powder X-ray diffraction measurements were performed on a PANalytical X’Pert PRO diffractometer equipped with a Cu K $\alpha$  radiation source ( $\lambda = 1.5418 \text{ \AA}$ ) in Bragg–Brentano geometry using a Si zero-background holder.

**Opening BNNTs:** To as-received BNNTs (100 mg, BNNT LLC, produced using the high-temperature high-pressure method) was added an aqueous solution of ammonium hydroxide (200 mL, 10% in water) and the suspension homogenized by tip ultrasonication (20 kHz, 130 W Sonics Vibracell CPX150 ultrasonic processor) for 4, 10, or 24 h at room temperature. Any visible clumps of BNNTs which had not dispersed were discarded. The resultant suspended gray/brown solid was collected by vacuum filtration (0.2  $\mu\text{m}$  PTFE membrane) and washed with deionized water (20 mL). This was further heated at 800 °C for 1 h, washed with hot ( $\approx 90 \text{ }^\circ\text{C}$ ) deionized water ( $\approx 500 \text{ mL}$ ) and collected by vacuum filtration (0.2  $\mu\text{m}$  PTFE membrane). Mass = 52 mg.

**Filling BNNTs:** Open and purified BNNTs (10 mg) and C<sub>60</sub>-fullerene (10 mg, SES Research) were sealed under vacuum (10<sup>-5</sup> mbar) in a Pyrex tube and heated at 600 °C for 20 h. The solid was collected by vacuum filtration (0.2  $\mu\text{m}$  PTFE membrane) and washed extensively with toluene until the filtrate became colorless. Mass = 8.2 mg.

**Formation of CNT@BNNT:** C<sub>60</sub>@BNNT (9.0 mg) was sealed under Ar (0.7 bar) in a quartz ampoule and heated at 1200 °C for 6 h. Mass = 7.1 mg.

## Supporting Information

Supporting Information is available from the Wiley Online Library or from the author.

## Acknowledgements

The authors would like to thank the European Research Council (ERC, NANOMOL), the Engineering and Physical Sciences Research Council (EPSRC, EP/L014696/1), and the University of Nottingham for financial support of this research. The authors thank Semilab Ltd. for the opportunity to use their UV Raman spectrometer. Á.P. acknowledges support of the Bolyai János Scholarship of the Hungarian Academy of Sciences and the support of the Hungarian National Research, Development, and Innovation Office through Grant No. NKFIH PD-121320. Research in Budapest was supported by the Hungarian National Research Fund (OTKA) through Grant No. NK 105691.

## Conflict of Interest

The authors declare no conflict of interest.

## Keywords

confinement, fullerenes, nanocontainers, nanoreactors, nanotubes

Received: May 9, 2017

Revised: June 15, 2017

Published online:

- [1] M.-F. Yu, O. Lourie, M. J. Dyer, K. Moloni, T. F. Kelly, R. S. Ruoff, *Science* **2000**, *287*, 637.
- [2] H. Dai, *Acc. Chem. Res.* **2002**, *35*, 1035.
- [3] J. W. G. Wilder, L. C. Venema, A. G. Rinzler, R. E. Smalley, C. Dekker, *Nature* **1998**, *391*, 59.
- [4] B. W. Smith, M. Monthieux, D. E. Luzzi, *Nature* **1998**, *396*, 323.
- [5] T. Okazaki, Y. Iizumi, S. Okubo, H. Kataura, Z. Liu, K. Suenaga, Y. Tahara, M. Yudasaka, S. Okada, S. Iijima, *Angew. Chem., Int. Ed.* **2011**, *50*, 4853.
- [6] B. Botka, M. E. Füstös, H. M. Tóháti, K. Németh, G. Klupp, Z. Szekrényes, D. Kocsis, M. Utczás, E. Székely, T. Váczi, G. Tarczay, R. Hackl, T. W. Chamberlain, A. N. Khlobystov, K. Kamarás, *Small* **2014**, *10*, 1369.
- [7] Y. K. Chen, A. Chu, J. Cook, M. L. H. Green, P. J. F. Harris, R. Heesom, M. Humphries, J. Sloan, S. C. Tsang, J. F. C. Turner, *J. Mater. Chem.* **1997**, *7*, 545.
- [8] P. M. Ajayan, T. W. Ebbesen, T. Ichihashi, S. Iijima, K. Tanigaki, H. Hiura, *Nature* **1993**, *362*, 522.
- [9] E. Dujardin, T. W. Ebbesen, H. Hiura, K. Tanigaki, *Science* **1994**, *265*, 1850.
- [10] J. Sloan, J. Hammer, M. Zwiefka-Sibley, M. L. H. Green, *Chem. Commun.* **1998**, 347.
- [11] Y. J. Dappe, *J. Phys. D: Appl. Phys.* **2014**, *47*, 083001.
- [12] A. N. Khlobystov, D. A. Britz, A. Ardavan, G. A. D. Briggs, *Phys. Rev. Lett.* **2004**, *92*, 245507.
- [13] D. A. Britz, A. N. Khlobystov, K. Porfyrakis, A. Ardavan, G. A. D. Briggs, *Chem. Commun.* **2005**, 37.
- [14] A. Botos, J. Biskupek, T. W. Chamberlain, G. A. Rance, C. T. Stoppiello, J. Sloan, Z. Liu, K. Suenaga, U. Kaiser, A. N. Khlobystov, *J. Am. Chem. Soc.* **2016**, *138*, 8175.
- [15] V. V. Chaban, O. V. Prezhdo, *ACS Nano* **2011**, *5*, 5647.
- [16] S. Campestrini, C. Corvaja, M. De Nardi, C. Ducati, L. Franco, M. Maggini, M. Meneghetti, E. Menna, G. Ruaro, *Small* **2008**, *4*, 350.
- [17] H. E. Lim, Y. Miyata, R. Kitaura, Y. Nishimura, Y. Nishimoto, S. Irle, J. H. Warner, H. Kataura, H. Shinohara, *Nat. Commun.* **2013**, *4*, 2548.
- [18] Y. Nakanishi, H. Omachi, N. A. Fokina, P. R. Schreiner, R. Kitaura, J. E. P. Dahl, R. M. K. Carlson, H. Shinohara, *Angew. Chem., Int. Ed.* **2015**, *54*, 10802.
- [19] S. Bandow, M. Takizawa, K. Hirahara, M. Yudasaka, S. Iijima, *Chem. Phys. Lett.* **2001**, *337*, 48.
- [20] G. Pagona, G. Rotas, A. N. Khlobystov, T. W. Chamberlain, K. Porfyrakis, N. Tagmatarchis, *J. Am. Chem. Soc.* **2008**, *130*, 6062.
- [21] C. S. Allen, Y. Ito, A. W. Robertson, H. Shinohara, J. H. Warner, *ACS Nano* **2011**, *5*, 10084.
- [22] A. Chuvilin, E. Bichoutskaia, M. C. Gimenez-Lopez, T. W. Chamberlain, G. A. Rance, N. Kuganathan, J. Biskupek, U. Kaiser, A. N. Khlobystov, *Nat. Mater.* **2011**, *10*, 687.
- [23] A. V. Talyzin, I. V. Anoshkin, A. V. Krasheninnikov, R. M. Nieminen, A. G. Nasibulin, H. Jiang, E. I. Kauppinen, *Nano Lett.* **2011**, *11*, 4352.
- [24] A. I. Chernov, P. V. Fedotov, A. V. Talyzin, I. S. Lopez, I. V. Anoshkin, A. G. Nasibulin, E. I. Kauppinen, E. D. Obraztsova, *ACS Nano* **2013**, *7*, 6346.
- [25] H. M. Ghassemi, R. S. Yassar, *Appl. Mech. Rev.* **2010**, *63*, 020804.
- [26] Y. Chen, J. Zou, S. J. Campbell, G. Le Caer, *Appl. Phys. Lett.* **2004**, *84*, 2430.
- [27] X. Blase, A. Rubio, S. G. Louie, M. L. Cohen, *Europhys. Lett.* **1994**, *28*, 335.
- [28] M. Terrones, J. M. Romo-Herrera, E. Cruz-Silva, F. Lopez-Urias, E. Munoz-Sandoval, J. J. Velazquez-Salazar, H. Terrones, Y. Bando, D. Golberg, *Mater. Today* **2007**, *10*, 30.
- [29] D. Golberg, Y. Bando, M. Mitome, K. Fushimi, C. Tang, *Acta Mater.* **2004**, *52*, 3295.



- [30] W. Han, P. Redlich, F. Ernst, M. Ruhle, *Appl. Phys. Lett.* **1999**, *75*, 1875.
- [31] W.-Q. Han, A. Zettl, *Appl. Phys. Lett.* **2002**, *81*, 5051.
- [32] Y. Bando, K. Ogawa, D. Golberg, *Chem. Phys. Lett.* **2001**, *347*, 349.
- [33] F.-F. Xu, Y. Bando, D. Golberg, M. Hasegawa, M. Mitome, *Acta Mater.* **2004**, *52*, 601.
- [34] D. Golberg, F.-F. Xu, Y. Bando, *Appl. Phys. A* **2003**, *76*, 479.
- [35] W.-Q. Han, C. W. Chang, A. Zettl, *Nano Lett.* **2004**, *4*, 1355.
- [36] T. Pham, A. Fathalizadeh, B. Shevitski, S. Turner, S. Aloni, A. Zettl, *Nano Lett.* **2016**, *16*, 320.
- [37] W. Mickelson, S. Aloni, W.-Q. Han, A. Zettl, *Science* **2003**, *300*, 467.
- [38] J. W. Kang, H. J. Hwang, *J. Phys. Condens. Matter* **2004**, *16*, 3901.
- [39] J. Wang, C. H. Lee, Y. K. Yap, *Nanoscale* **2010**, *2*, 2028.
- [40] P. Singla, N. Goel, V. Kumar, S. Singhal, *Ceram. Int.* **2015**, *41*, 10565.
- [41] Q. Weng, X. Wang, X. Wang, Y. Bando, D. Golberg, *Chem. Soc. Rev.* **2016**, *45*, 3989.
- [42] Y. Liao, Z. Chen, J. W. Connell, C. C. Fay, C. Park, J.-W. Kim, Y. Lin, *Adv. Funct. Mater.* **2014**, *24*, 4497.
- [43] C. H. Lee, D. Zhang, Y. P. Yap, *J. Phys. Chem. C* **2012**, *116*, 1798.
- [44] C. Zhi, N. Hanagata, Y. Bando, D. Golberg, *Chem. Asian J.* **2011**, *6*, 2530.
- [45] H. Chen, Y. Chen, J. Yu, J. S. Williams, *Chem. Phys. Lett.* **2006**, *425*, 315.
- [46] D. Golberg, Y. Bando, Y. Huang, T. Terao, M. Mitome, C. Tang, C. Zhi, *ACS Nano* **2010**, *4*, 2979.
- [47] D. Golberg, Y. Bando, C. C. Tang, C. Y. Zhi, *Adv. Mater.* **2007**, *19*, 2413.
- [48] P. Kondratyuk, J. T. Yates, *J. Am. Chem. Soc.* **2007**, *129*, 8736.
- [49] L. A. Girifalco, M. Hodak, R. S. Lee, *Phys. Rev. B* **2000**, *62*, 13104.
- [50] H. Ulbricht, G. Moos, T. Hertel, *Phys. Rev. Lett.* **2003**, *90*, 095501.
- [51] K. S. Troche, V. R. Coluci, S. F. Braga, D. D. Chinellato, F. Sato, S. B. Legoas, R. Rurali, D. S. Galvao, *Nano Lett.* **2005**, *5*, 349.
- [52] J. H. Warner, Y. Ito, M. Zaka, L. Ge, T. Akachi, H. Okimoto, K. Porfyrakis, A. A. R. Watt, H. Shinohara, G. A. D. Briggs, *Nano Lett.* **2008**, *8*, 2328.
- [53] K. Berland, P. Hyldgaard, *Phys. Rev. B* **2013**, *87*, 205421.
- [54] P. A. Heiney, J. E. Fischer, A. R. McGhie, W. J. Romanow, A. M. Denenstien, J. P. McCauley, A. B. Smith, D. E. Cox, *Phys. Rev. Lett.* **1991**, *66*, 2911.
- [55] P. A. Heiney, *J. Phys. Chem. Solids* **1992**, *53*, 1333.
- [56] Á. Pekker, G. Németh, A. Botos, H. M. Tóháti, F. Borondics, Z. Osváth, L. P. Biró, K. Walker, A. N. Khlobystov, K. Kamarás, *Phys. Status Solidi B* **2016**, *253*, 2457.
- [57] B. Fakrach, A. Rahmani, H. Chadli, K. Sbai, M. Bentaleb, J.-L. Bantignies, J.-L. Sauvajol, *Phys. Rev. B* **2012**, *85*, 115437.
- [58] C. H. Lee, M. Xie, V. Kayastha, J. Wang, Y. K. Yap, *Chem. Mater.* **2010**, *22*, 1782.
- [59] K. Kamarás, L. Akselrod, S. Roth, A. Mittelbach, W. Hönle, H. G. von Schnering, *Chem. Phys. Lett.* **1993**, *214*, 338.
- [60] R. A. Jishi, R. M. Mirie, M. S. Dresselhaus, *Phys. Rev. B* **1992**, *45*, 13685.
- [61] S. Pekker, É. Kováts, G. Oszlányi, G. Bényei, G. Klupp, G. Bortel, I. Jalsovszky, E. Jakab, F. Borondics, K. Kamarás, M. Bokor, G. Kriza, K. Tompa, G. Faigel, *Nat. Mater.* **2005**, *4*, 764.
- [62] D. S. Bethune, G. Meijer, W. C. Tang, H. J. Rosen, W. G. Golden, H. Seki, C. A. Brown, M. S. de Vries, *Chem. Phys. Lett.* **1991**, *179*, 181.
- [63] R. Pfeiffer, H. Kuzmany, T. Pichler, H. Kataura, Y. Achiba, M. Melle-Franco, F. Zerbetto, *Phys. Rev. B* **2004**, *69*, 035404.
- [64] F. Simon, H. Peterlik, R. Pfeiffer, J. Bernardi, H. Kuzmany, *Chem. Phys. Lett.* **2007**, *445*, 288.
- [65] L. Jing, R. Y. Tay, H. Li, S. H. Tsang, J. Huang, D. Tan, B. Zhang, E. H. T. Teo, A. I. Y. Tok, *Nanoscale* **2016**, *8*, 11114.
- [66] C. Y. Su, Z. Y. Juang, Y. L. Chen, K. C. Leou, C. H. Tsai, *Diamond Relat. Mater.* **2007**, *16*, 1393.
- [67] Y. Morihisa, C. Kimura, M. Yukawa, H. Aoki, T. Kobayashi, S. Hayashi, S. Akita, Y. Nakayama, T. Sugino, *J. Vac. Sci. Technol., B* **2008**, *26*, 872.
- [68] M. Mohai, I. Mohai, Z. Sebestyén, A. Gergely, P. Németh, J. Szépvölgyi, *Surf. Interface Anal.* **2010**, *42*, 1148.
- [69] Y. J. Jeong, M. F. Islam, *Nanoscale* **2015**, *7*, 12888.
- [70] X. Yang, Z. Li, F. He, M. Liu, B. Bai, W. Liu, X. Qiu, H. Zhou, C. Li, Q. Dai, *Small* **2015**, *11*, 3710.
- [71] W.-L. Wang, J.-Q. Bi, W.-X. Sun, H.-L. Zhu, J.-J. Xu, M.-T. Zhao, Y.-J. Bai, *Mater. Chem. Phys.* **2010**, *122*, 129.
- [72] L. Chen, H. Ye, Y. Gogotsi, *J. Am. Ceram. Soc.* **2004**, *87*, 147.
- [73] D. R. Kauffman, A. Star, *Angew. Chem., Int. Ed.* **2008**, *47*, 6550.
- [74] R. Arenal, A. Lopez-Bezanilla, *ACS Nano* **2014**, *8*, 8419.
- [75] B. W. Smith, D. E. Luzzi, *Chem. Phys. Lett.* **2000**, *321*, 169.
- [76] R. Pfeiffer, M. Holzweber, H. Peterlik, H. Kuzmany, Z. Liu, K. Suenaga, H. Kataura, *Nano Lett.* **2007**, *7*, 2428.
- [77] R. F. Egerton, *Rep. Prog. Phys.* **2009**, *72*, 016502.
- [78] Z. Zhang, W. Guo, G. Tai, *Appl. Phys. Lett.* **2007**, *90*, 133103.
- [79] G. A. Rance, D. H. Marsh, R. J. Nicholas, A. N. Khlobystov, *Chem. Phys. Lett.* **2010**, *493*, 19.